


Article

# Investigation of Collagen-Incorporated Sodium Alginate Bioprinting Hydrogel for Tissue Engineering

Yan Chen, Yingge Zhou \*  and Chi Wang

Systems Science and Industrial Engineering, Binghamton University, Binghamton, NY 13901, USA

\* Correspondence: yzhou@binghamton.edu; Tel.: +1-607-777-5015

**Abstract:** Tissue engineering is a promising area that is aimed at tissue regeneration and wound repair. Sodium alginate (SA) has been widely used as one of the most biocompatible materials for tissue engineering. The cost-efficiency and rapid gel ability made SA attractive in wound healing and regeneration area. To improve printability and elasticity, many hydrogel-based bioinks were developed by mixing SA with other natural or synthetic polymers. In this paper, composite SA/COL bioink was used for the bioprinting of artificial cartilage tissue mimics. The results showed that the concentration of both SA and COL has significant effects on filament diameter and merging. A higher concentration of the bioink solution led to better printing fidelity and less deformation. Overall, a higher SA concentration and a lower COL concentration contributed to a lower shrinkage ratio after crosslinking. In summary, the SA/COL composite bioink has favorable rheological properties and this study provided material composition optimization for future bioprinting of engineered tissues.

**Keywords:** bioprinting; sodium alginate; collagen; tissue engineering



**Citation:** Chen, Y.; Zhou, Y.; Wang, C. Investigation of Collagen-Incorporated Sodium Alginate Bioprinting Hydrogel for Tissue Engineering. *J. Compos. Sci.* **2022**, *6*, 227.  
<https://doi.org/10.3390/jcs6080227>

Academic Editor: Francesco Tornabene

Received: 28 June 2022

Accepted: 2 August 2022

Published: 4 August 2022

**Publisher's Note:** MDPI stays neutral with regard to jurisdictional claims in published maps and institutional affiliations.



**Copyright:** © 2022 by the authors. Licensee MDPI, Basel, Switzerland. This article is an open access article distributed under the terms and conditions of the Creative Commons Attribution (CC BY) license (<https://creativecommons.org/licenses/by/4.0/>).

## 1. Introduction

Tissue engineering has gained plenty of attention in recent years. It is a major technique in regenerative medicine that produces biological substitutes for tissue regeneration and repairing [1]. The additive manufacturing techniques fabricate tissues or organ prototypes by digital control to realize precise printing of tissue scaffolds with biocompatible materials such as polycaprolactone (PCL) [2]. Furthermore, combining 3D printing and bioprinting allows for the fabrication of detailed structure loading with homogeneously distributed cells possible [3]. Since the ultimate goal of engineered tissues is to replace native tissues and organs, the biomaterials for tissue scaffold fabrication should be highly biocompatible and biodegradable. Alternatively, considerable mechanical strength is often desirable to support cell proliferation and tissue formation. Therefore, it is challenging to reach a balance between structural integrity and material biocompatibility.

Natural polymers such as gelatin, alginate, hyaluronic acid, and chitosan are often used as bioprinting materials owing to their low toxic and biodegradable properties [4]. Among these natural polymers, the rapid biodegradability and chemical gelling capability of alginate make it attractive in artificial extracellular matrix (ECM) fabrication [5]. Due to the water retention property and tissue-like softness, bioprinting of SA hydrogel is widely applied in soft tissue engineering applications such as skin and cartilage regeneration for enhanced cell attachment and proliferation [6,7]. Alternatively, despite the cell-friendly environment provided by SA hydrogel, the structural integrity and printing fidelity of bioprinted SA hydrogel are often compromised due to the limited mechanical strength and elasticity. Pure SA hydrogel cannot store enough energy to maintain its structure, which lead to poor rheological behavior [8]. In this case, several strategies were put forward to solve this issue.

One of the solutions was combining other fabrication techniques, such as electrospinning with 3D printing. For example, An et al. took an electrospinning mat as the basement

to improve mechanical strength and trap cells [9]. Another strategy was to transform the natural polymers into sol-gel states by crosslinking [10]. The combination of ionic and covalent bonds linked two or more polymeric chains and formed a long molecule [11]. Therefore, the crosslinked hydrogel can provide higher inner supportiveness to maintain structure. Some researchers rose the printability of hydrogel by mixing SA with various synthesis or natural polymers. For example, sodium alginate–gelatin hydrogel is one of the most often used composite bioink for bioprinting with high cell viability and printability [12–14]. In other studies, blended SA with poly (vinyl alcohol) (PVA) also showed an increase in supportiveness and stability of scaffolds [15,16]. Kumar et al. took advantage of carboxylated cellulose nanocrystals and xanthan gum to improve the rheological behavior and obtained good printability [17].

Collagen is another natural material that is often used as bioprinting hydrogel besides gelatin. Collagen is the major protein content in ECM and connective tissue such as cartilage [18]. Similar to sodium alginate, the collagen hydrogel is highly biocompatible but has a lack of mechanical strength [19], which indicates it could be difficult to maintain the structure of the collagen printed scaffold. One way to resolve this challenge was to print collagen bioink with supportive hydrogel. For example, Isaacson et al. utilized four types of collagen mixed with SA as scaffolds for artificial corneal, and collagen type I showed the best quality and stability [20]. Wu et al. printed cell-laden collagen/gelatin/alginate hydrogel and achieved a stable structure with high cell viability [21]. In another study, Yang et al. combined collagen type I (COL) with SA to construct cartilage tissue for enhanced mechanical strength. The SA/COL scaffold showed improved mechanical strength and great expression of cartilage-specific genes [22]. However, few studies have investigated how the concentration change of SA and COL hydrogel changes the mechanical and rheological properties of the composite hydrogel, thus altering the printability and shape fidelity of the printed scaffolds.

In this paper, we investigated the effects of the concentration on SA/COL composite hydrogel for potential cartilage tissue engineering applications. The objective of this study is to investigate the effects of SA and COL concentration on bioink printability and shape fidelity. The hypothesis is that the addition of COL into SA hydrogel in various concentrations will alter the rheological properties of the printing hydrogel, therefore changing the printability of the bioink. To test this hypothesis, three SA concentrations and three COL concentrations were selected to obtain nine composite bioink groups with tunable rheological properties. After bioprinting,  $\text{CaCl}_2$  crosslinking solution was added to improve scaffolds' structural integrity. Rheometer, optical microscope, and FTIR were used for characterizations. Statistical analysis on filament extrusion and merging was also conducted to assess filament extrusion consistency and filament merging effects. The results showed that the SA and COL concentration has a significant influence on filament diameter, merged filament size, and solution viscosity.

## 2. Materials and Methods

### 2.1. Solution Preparation

Sodium Alginate (SA) powder was purchased from SIGMA-ALDRICH, Co. (St. Louis, MO, USA). Collagen (COL) powder was purchased from Doctor's Best, Inc. (Irvine, CA, USA). Calcium Chloride Anhydrous pellets were purchased from Fisher Scientific, Co. (Fair Lawn, NJ, USA). Deionized water (DI water) was obtained from a Millipore Milli-Q system.

The 7%, 8%, and 9% SA with 0%, 1%, and 2% COL solutions were prepared by dissolving sodium alginate powder and collagen powder in DI water through magnetic stirring for 24 h at 50 °C (Figure 1). Nine SA/COL solutions were prepared for the experiment. The concentration ratios were selected based on preliminary experimental results. The 1%  $\text{CaCl}_2$ /DI water solution was prepared by dissolving calcium chloride anhydrous pellets in DI water and stirring for 5 min.

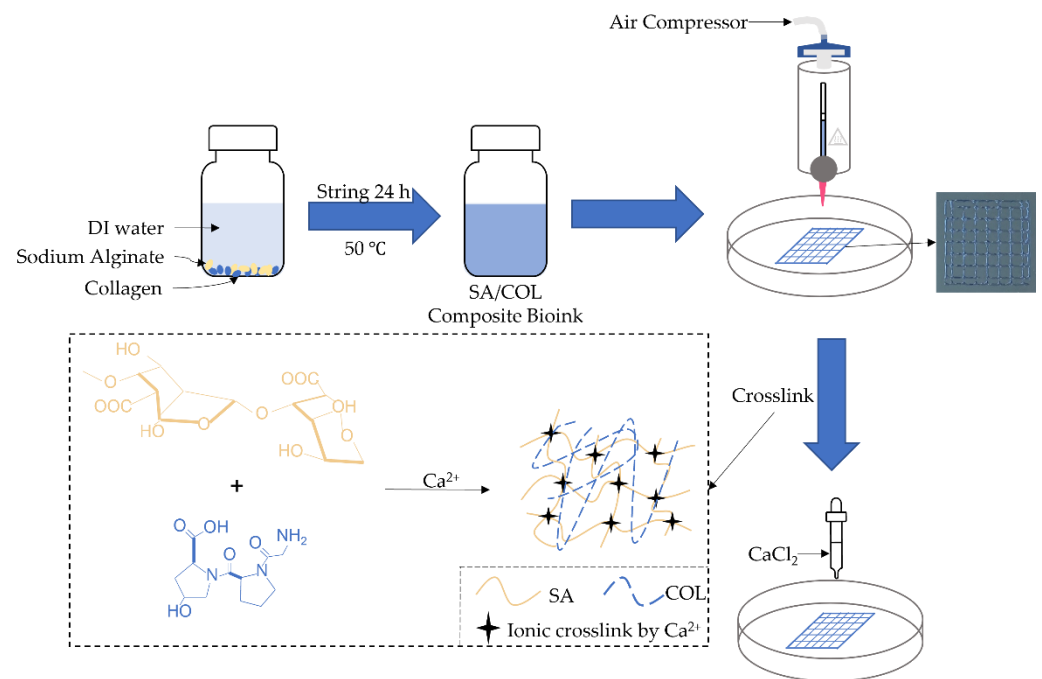


**Figure 1.** Schematic illustration of the bioprinting process.

### 2.2. Fourier Transform Infrared (FT-IR) Spectroscopy

The FT-IR analysis was conducted by a Nicolet 8700 FTIR spectrometer from Thermo Fisher Scientific (Waltham, MA, USA). The Attenuated Total Reflectance (ATR) mode was used with a Germanium plate and MCT/A detector. Nine hydrogel solutions were loaded separately, and the spectrum data were collected after baseline correction.

### 2.3. Rheological and Viscosity Measurements

The rheological and viscosity measurements were completed by Discovery HR 30 Rheometer (Waters, Milford, MA, USA). Oscillation frequencies were conducted by altering angular frequency from 0.1 rad/s to 100.0 rad/s at a fixed strain of 1.0%. The samples were also subjected to flow sweeps ranging from 1.0 1/s to 100.0 1/s to study their shear stress and viscosities. The temperature was fixed at 25 °C and the soak time was 180.0 s for both procedures.

### 2.4. Bioprinting Process

The printing process was performed on a BIO X printer (Cellink, Virginia, USA) with a 25 kPa pressure. The composite bioinks were extruded from a syringe connected to an air compressor with a 0.25 mm nozzle diameter. Filament square frames and  $20 \times 20 \times 0.25$  mm grids were printed with 15% infill density and 10 mm/s scanning speed (Figure 1). Five square frames and five grids were printed for each group.

### 2.5. Characterization of Printed Frame and Grids

The printed samples were first observed using EVOS XL Core optimal microscope (Thermo Fisher Scientific Inc., Waltham, MA, USA). The frames and grids were then crosslinked by dropping 1%  $\text{CaCl}_2$  solution onto the printed constructs until they were fully immersed. After five minutes of crosslinking, the samples were observed using an optical microscope again.

Filament diameters, merged filament sizes, and mesh areas were measured by ImageJ (National Institutes of Health, Bethesda, MD, USA). The upper line and bottom line of each square frame were taken as filament observations. Two points (point A and point B) with a distance of 2 mm were picked randomly from each sample for four-width measurement (Figure 2a). Two grid cells were randomly picked from each sample for four diagonal mea-

measurements (Figure 2b) and two mesh area measurements (Figure 2c). Thirty measurements were conducted for each group for filament diameter, merging, and mesh area.

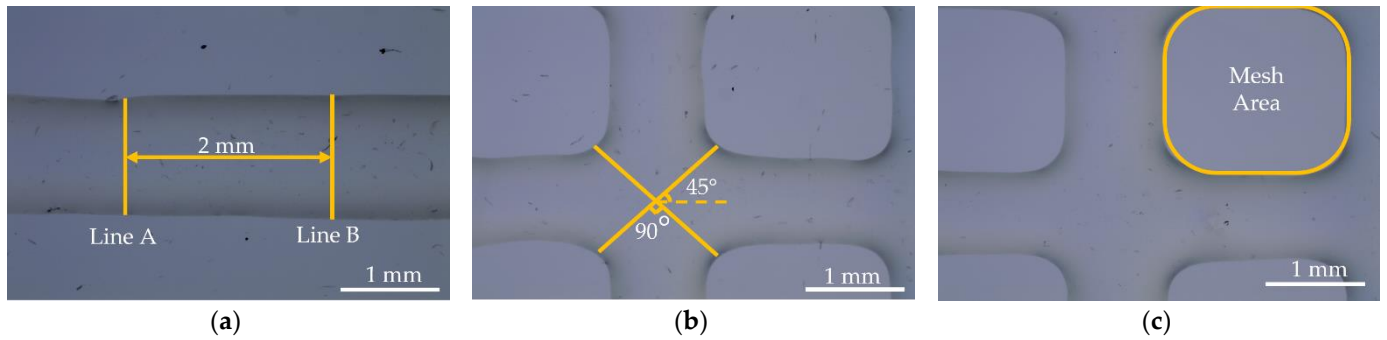


Figure 2. Measurement of (a) filament diameter, (b) merged filament size, (c) and mesh area.

### 3. Results

#### 3.1. Rheometer

The log scale of storage modulus ( $G'$ ) and loss modulus ( $G''$ ) of different SA concentrations are shown in Figure 3 for better visibility. The figures showed that the 9%SA1%COL, 8%SA2%COL, and 7%SA1%COL have similar  $G'$  and  $G''$  and that they were higher than other groups. Therefore, the samples printed through these three groups have the higher internal strength to maintain their structure. Vice versa, the hydrogels with lower concentration (7%SA0%COL and 7%SA2%COL) have the lowest  $G'$  and  $G''$ , which lead to the liquid-like bioinks and may not have held their shape very well in certain circumstances. All nine groups showed higher  $G'$  compared to  $G''$ , except for 7%SA0%COL and 7%SA2%COL (when the angular frequency was higher than 0.63 rad/s). This indicated most of our composite bioink groups were suitable for bioprinting, as the printed shape would be held, while still being able to be extruded.

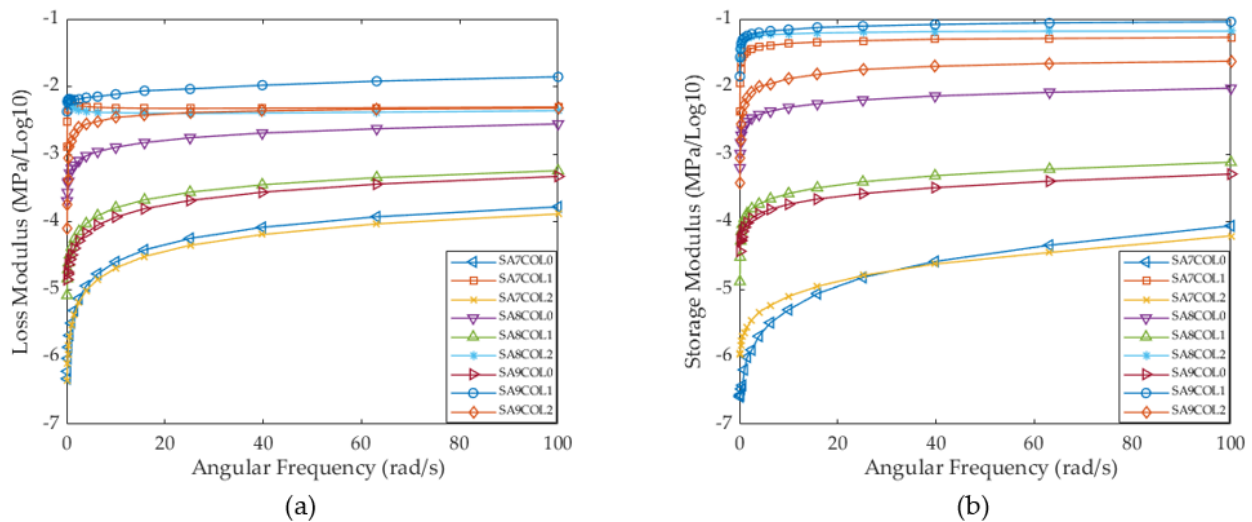


Figure 3. (a) Storage modulus ( $G'$ ) and (b) loss modulus ( $G''$ ).

The log scale of viscosity-shear rate curves (Figure 4a) showed that viscosity for all groups decreased with the increase in shear rate, indicating the composite bioinks were shear-thinning fluids. The log scale of the shear stress-shear rate curve in Figure 4b showed increased trends, which testified that all groups of bioinks exhibited shear-thinning properties. Although, when the overall viscosity increased by adding more SA and COL, the shear-thinning property was less evident in the lower shear rate range. Nevertheless,

this indicated that the SA/COL composite bioinks were suitable for bioprinting with favorable rheological properties.

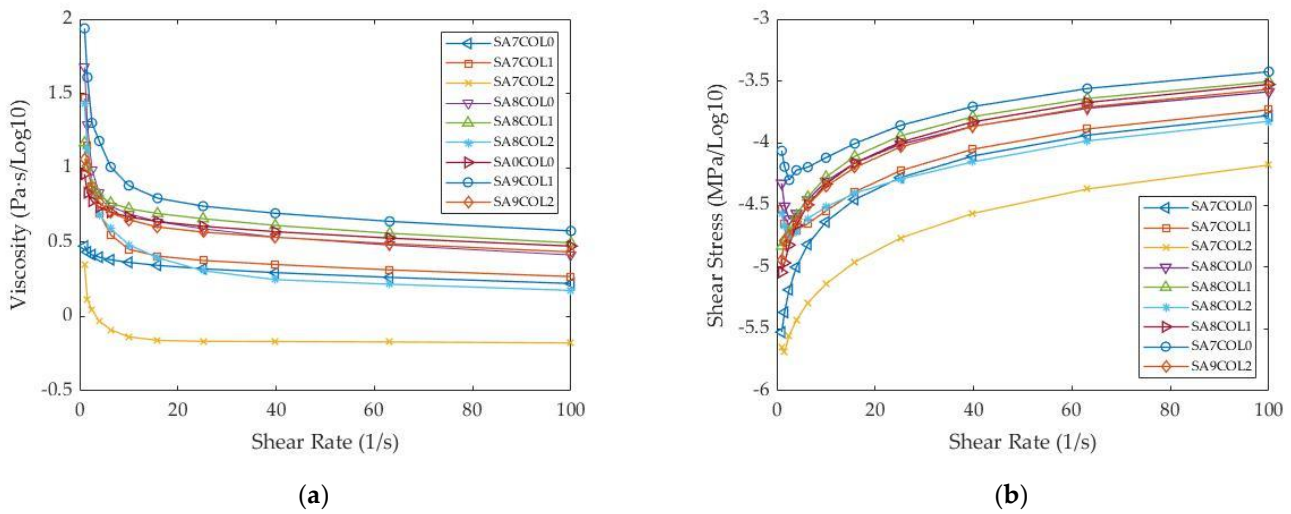


Figure 4. (a) Viscosity-shear rate curve; (b) Shear stress-shear rate curve.

### 3.2. FTIR

To characterize the chemistry of the SA/COL blends, we analyzed the hydrogels by using FT-IR. As shown in Figure 5, the highest peak at around  $3375\text{ cm}^{-1}$  was due to the alcohol's phenols (O-H) stretching, which was common in other hydrogel solutions. The two absorption peaks at  $1640\text{ cm}^{-1}$  and  $1414\text{ cm}^{-1}$  were owing to asymmetric stretching by nitro compound (N-O) and stretching by amide (C=O). The ether bond (C-O) stretching vibration led to the peak at  $1010\text{ cm}^{-1}$  and  $1032\text{ cm}^{-1}$ . Since the peaks of different solutions were similar, adding COL into the SA solution did not significantly change the hydrogen bond interaction and spectrum absorption, with only a small variation between  $1000\sim 1200\text{ cm}^{-1}$  wavelength. Alternatively, the addition of both SA and COL increased the number of ether bonds, leading to a higher peak than a low concentration solution.

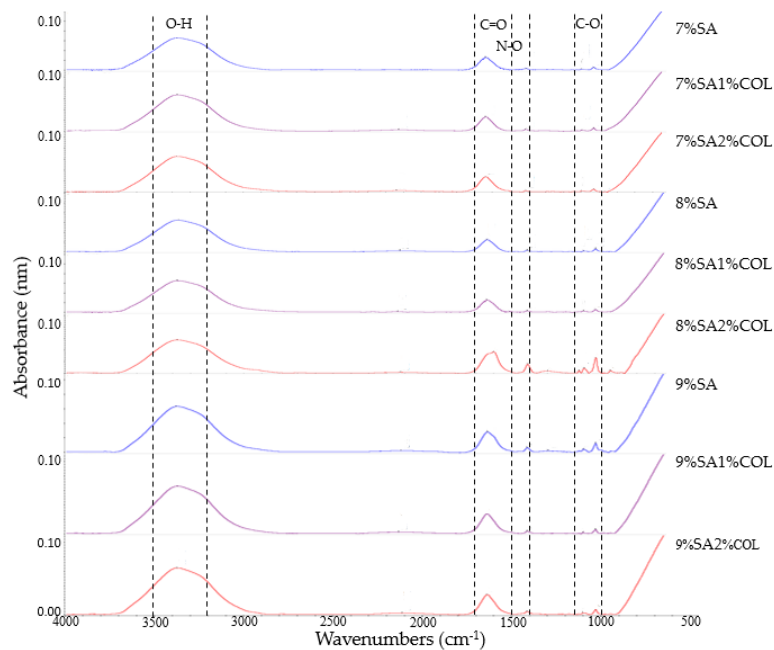
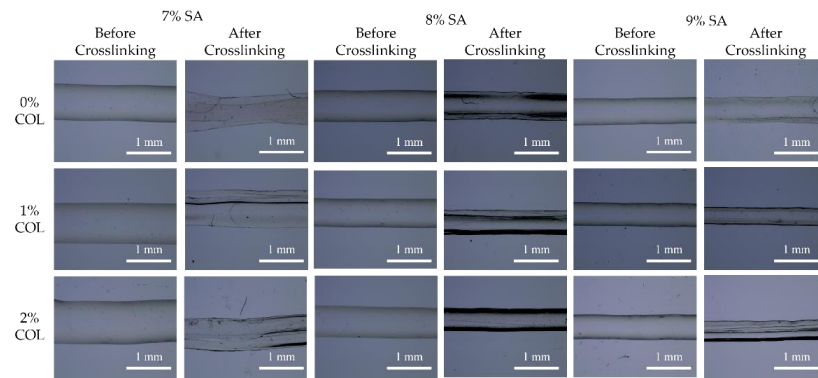


Figure 5. FT-IR for SA/COL solutions.



### 3.3. Printed Filament

The optical microscope images of printed filaments in Figure 6 showed that the filament diameter seemed to be decreased in higher SA/COL concentration groups before crosslinking. After crosslinking, some of the groups showed distinct layered sections, while some did not. All nine groups were observed with shrinkage in filament size after crosslinking.



**Figure 6.** Images of filament before and after crosslink.

After filament measurements, Minitab was used to analyze the statistical significance. Table 1 listed the average filament diameter and shrinkage ratio after crosslinking and the *p* values with COL and SA concentration levels as factors, respectively. The filament diameter decreased with the increase in SA concentration. Alternatively, the increasing trend within the same SA concentration group changed with different COL, indicating there were interactive effects from both SA and COL. After crosslinking, the overall standard deviation of filament diameter increased, showing that the crosslinking process significantly influenced the uniformity of the filament. From the *p*-values of filament diameter analysis, it was evident that both COL and SA concentration had significant effects (except for 7% SA groups after crosslinking) on the filament diameter and the shrinkage ratio increased with higher COL concentration and lower SA concentration.

**Table 1.** Statistical analyses for filament diameter.

Filament Diameter before and after Crosslinking (mm)									
Filament diameter	7% SA			8% SA			9% SA		
	0% COL	1% COL	2% COL	0% COL	1% COL	2% COL	0% COL	1% COL	2% COL
Before crosslinking	1.168	1.281	1.432	1.006	0.945	1.009	0.849	0.638	0.790
After crosslinking	1.005	0.942	0.917	0.887	0.638	0.704	0.804	0.418	0.497
Shrinkage ratio	13.96%	26.46%	35.96%	11.83%	32.49%	30.23%	5.30%	34.48%	37.09%
<i>p</i> -Values of Filament Diameter Analysis (Factor = COL)									
Diameter Average	Status			7% SA	8% SA	9% SA			
	Before crosslinking			0.000 ***	0.000 ***	0.000 ***			
After crosslinking			0.367	0.000 ***	0.000 ***				
<i>p</i> -Values of Filament Diameter Analysis (factor = SA)									
Diameter Average	Status			0% COL	1% COL	2% SA			
	Before crosslinking			0.000 ***	0.000 ***	0.000 ***			
After crosslinking			0.000 ***	0.000 ***	0.000 ***				

(\*\*\* stands for *p* < 0.001).

### 3.4. Filament Merging

The optical microscope images of filament merging in Figure 7 showed that the merged filament shape changed from a round-like to a square-like shape with the increase of SA/COL bioink concentration. Although it seemed that the COL concentration had fewer effects on the merged filament shape. Instead, circular grid size in 7% SA groups decreased with higher COL concentration, indicating more deformation. Similar to filament diameter, all nine groups showed shrinkage in merged filament size after crosslinking. However, no obvious layered structures were observed.

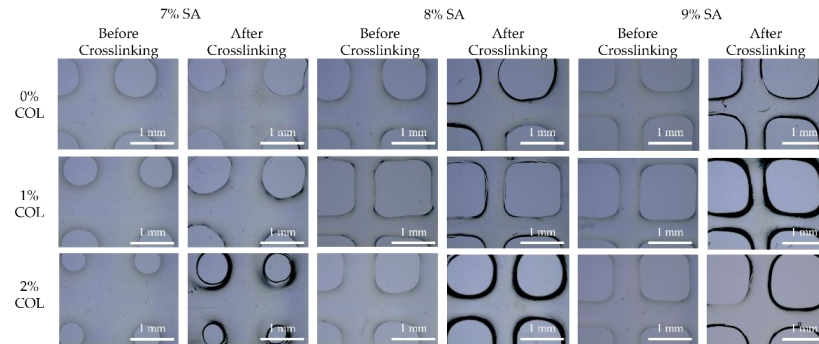


**Figure 7.** Images of printed grids before and after crosslinking.

Table 2 showed the merged filament size, as well as the shrinkage ratio after crosslinking. In general, the merged filament size decreased with the increase of SA concentration and the shrinkage ratio increased with higher COL concentration and lower SA concentration. Similar to filament diameter, the increasing trend within the same SA concentration groups changed with different COL concentrations, indicating there were interactive effects from both SA and COL. After crosslinking, the overall standard deviation of filament diameter increased, showing that the crosslinking process significantly influences the uniformity of the filament. The ANOVA results showed that COL concentration did not have a significant influence on grid shape within 7% SA groups. The concentration of SA had a significant influence on filament merging before and after crosslinking.

**Table 2.** Statistical analyses for merged filaments.

		Filament Diameter before and after Crosslinking (mm)								
		7% SA			8% SA			9% SA		
Filament diameter		0% COL	1% COL	2% COL	0% COL	1% COL	2% COL	0% COL	1% COL	2% COL
Before crosslinking		2.670	2.651	2.852	2.160	2.114	2.120	1.701	1.538	1.758
After crosslinking		2.616	2.333	2.444	2.026	1.692	1.906	1.688	1.407	1.396
Shrinkage ratio		2.02%	12.00%	14.31%	6.20%	19.96%	10.09%	0.76%	8.52%	20.59%
		<i>p</i> -Values of Filament Diameter Analysis (Factor = COL)								
		Status		7% SA	8% SA	9% SA				
Diameter Average	Before crosslinking			0.136	0.036 *	0.000 ***				
	After crosslinking			0.063	0.000 ***	0.000 ***				
		<i>p</i> -Values of Filament Diameter Analysis (Factor = SA)								
		Status		0% COL	1% COL	2% SA				
Diameter Average	Before crosslinking			0.000 ***	0.000 ***	0.000 ***				
	After crosslinking			0.000 ***	0.000 ***	0.000 ***				

(\* stands for  $p < 0.05$ ; \*\*\* stands for  $p < 0.001$ ).

The mesh area was measured to present the shape fidelity of different groups. The ratio of printed mesh area to designed mesh area was shown in Figure 8. The boxplot showed that the shape fidelity of meshes improved by increasing SA concentration. Similar to filament merging, adding COL has interactive effects on mesh areas.

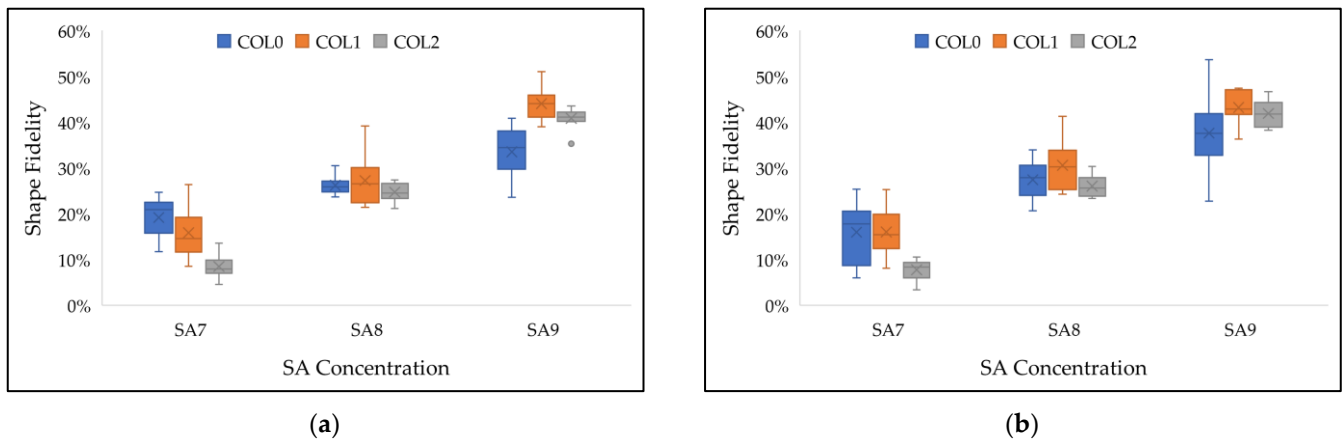


**Figure 8.** Boxplot of the percentage of measurement mesh area compared to designed 3D model (a) before crosslinking, and (b) after crosslinking.

#### 4. Discussion

Articular cartilage, an avascular tissue, has a limited spontaneous repair ability, which is a challenge for tissue regeneration that needs to be addressed. In clinical therapy, many approaches have been applied to cartilage defects treatment, such as microfracture [23], osteochondral autologous transplantation [24], and autologous chondrocyte implantation [25]. However, these treatments still have significant drawbacks, such as body rejection and infection for cartilage reconstruction [26]. Therefore, additive manufacturing was put forward as the novel method for artificial tissue manufacturing. Fused deposition manufacturing (FDM) [27], bioprinting [28], digital light processing (DLP) [29], and selective laser sintering (SLS) [30] are four techniques that are commonly used to generate cartilage-mimic tissue.

Although DLP and SLS allow for high resolution and can obtain precise scaffold structure, the usable materials are limited [31], and the manufacturing cost is higher than FDM. Moreover, bioprinting is often utilized for cell loading to increase cell attachment. Given the low accuracy of the printed scaffold by conventional bioinks, Rathana et al. extruded cECM (cartilage extracellular matrix)-functionalized bioink into 3D-printed PCL scaffold networks for better supportiveness [32]. Alternatively, researchers tried to reinforce the internal support of bioink by blending different hydrogel solutions or pre-crosslinking. Among these studies, sodium alginate, gelatin, and collagen were the most used materials to produce artificial cartilage tissue, and  $\text{CaCl}_2$  was applied for crosslinking [33–35]. Yang et al. compared the mechanical properties and biological functionality of pure SA, SA/agarose, and SA/COL. The results revealed that the SA/COL group had the best mechanical strength and benefit for phenotype preservation [22]. Furthermore, high concentrations of collagen-based bioink contribute to printing accuracy [36].

In this paper, we bioprinted composite SA/COL bioinks with various concentration ratios and crosslinked the printed constructs by dropping 1%  $\text{CaCl}_2/\text{DI}$  water solution. By utilizing an extrusion-based bioprinter, the composite SA/COL bioinks were extruded from the syringe nozzle by compressed air for a layer-by-layer process. Since the bioinks were hydrogels with low viscosity, it was important to investigate the printability and shape fidelity of the bioprinting process. Therefore, filament formation and merging effects were investigated. The rheological properties and material composition were also studied to better understand the effects on printability. In this study, the filament diameter before crosslinking ranged from 0.706–1.432 mm with the designed diameter of 0.25 mm. The filament merging measured as grid diagonal length ranged from 1.396 mm to 2.852 mm



with the designed size of 0.35 mm. Both filament diameter and filament merging showed shrinkage after crosslinking with  $\text{CaCl}_2/\text{DI}$  water solution. The shrinkage rate ranged from 5.3% to 37.09% for filament diameter and from 0.76% to 20.59% for filament merging. The results also showed that both SA and COL concentration had significant effects on filament diameter and filament merging. Indicating the printability and shape fidelity of printed scaffolds could be improved by changing the composition of SA/COL bioink.

Behind the effects of bioink composition on the printed filament, the significant effects it had on rheological properties, such as storage modulus, loss modulus, shear stress, and viscosity were the fundamental reasons in the materials science perspective. The  $G'$  and  $G''$  showed two aspects of solution viscosity. Higher  $G'$  indicated that it required larger energy to distort the shape of samples. Higher  $G''$  has the ability to store more energy elastically [8]. Therefore, if  $G'$  was greater than  $G''$ , the solution was more solid-like. On the contrary, if  $G'$  was less than  $G''$ , the solution was more liquid-like. As we can see in Figure 3, most groups have higher  $G'$  compared to  $G''$ . As shown in Figure 4, the viscosity increased with the increase of SA concentration, especially when the shear rate increased from 10 to 100 1/s. In Figure 4b, the log scale of the shear stress-shear rate curve showed a linear relationship after 2.51 1/s shear rate for most groups, which showed Bingham's pseudoplastic behavior and indicated a shear-thinning effect [37]. Although when the overall viscosity increased by adding more SA and COL, the shear-thinning property was less evident in the lower shear rate range. This indicated lower overall viscosity of the bioink and shear rate contribute to the shear-thinning effects. In terms of solution characteristics and material composition, the FT-IR results showed that the nine groups had similar spectrum absorption peaks, indicating an insignificant change in internal molecular structure (Figure 5). Therefore, it was safe to say both SA and COL concentrations had no significant effects on the internal molecular structure of the composite bioinks.

From Figures 6 and 7 we can see that the bioprinting processes obtained consistent extrusion of filaments over repetitions, indicating good printability. Alternatively, the filament diameter and merged filament size varied for different groups before and after crosslinking. The statistical analyses showed that both filament diameter and merged filament width increased compared to the designed size in the 3D model. This was consistent with other research that bioprinted hydrogel results in filament fusion and collapsing in general due to the low viscosity and mechanical strength [38,39].

In the ANOVA analysis, both COL and SA concentration had significant effects on filament diameter before and after crosslinking (Table 1). However, COL became an insignificant factor within 7% of SA groups after crosslinking. One possible explanation was that with lower zero-shear viscosity, the flow and deformation of the material will be higher, thus diminishing the effects of COL [40]. This was also tested by the high standard deviation (SD) of filament diameter in the 7% SA groups. Furthermore, with the increase in COL concentration, the shrinkage rate after crosslinking seemed to be increasing in all three SA groups. This could be attributed to the intrinsic of free calcium ions with high mobility to complexation with  $-\text{COOH}$  to form the crosslinking [41]. Besides, it was proved that the swelling response was not statistically significant for crosslink hydrogels at  $\text{pH} = 5$  [42]. With the increase of COL concentration, the  $\text{pH}$  value of hydrogel solution gradually increases and induced to higher shrinkage rate. When the COL concentration was low, the calcium ions react with SA rapidly and thus have less chance to penetrate the filament, forming a two-layer structure. With increasing COL concentration, more calcium ions were able to penetrate the filament, which resulted in a more uniform crosslinking (Figure 6).

Similar to filament diameter, both COL and SA concentration had significant effects on filament merging before and after crosslinking (Table 2). The only exception was with 7% SA groups, COL had no significant effects before crosslinking. This could also be explained by the higher flow and deformation of the bioink in lower zero-shear viscosity [31]. Due to the inhomogeneous shrinking process, the overall SD after crosslinking was larger than that before crosslinking [43]. Furthermore, the groups with a lower COL ratio seem to have less shrinkage. The 9%SA1%COL group resulted in merged filament size with the

least deformation. Alternatively, with lower SA concentration, the merged filament size increased with the increase of COL. However, when the SA concentration increased from 7% to 9%, the merged filament size decreased when COL concentration was 1%, but then increased when COL concentration was 2% (Figure 7). This mixed result indicated COL and SA concentration had interactive effects on merged filament size.

## 5. Conclusions

In summary, this study investigated the effects of composite SA/COL hydrogel composition on printability and shape fidelity for potential cartilage tissue engineering applications. The results showed that both SA and COL concentration had significant effects on filament diameter and merging. A higher concentration of the bioink solution led to better printing fidelity and less deformation. Overall, higher SA concentration and lower COL concentration contributed to a lower shrinkage ratio after crosslinking. However, maintaining the structure of pure SA, especially with low concentration, during the printing process was still a challenge that needs to be addressed. The results from this study provide a reference for bioink composition for potential tissue engineering applications such as artificial skin or cartilage tissues. Future work includes the bioprinting of cartilage biomimicry constructs by loading chondrocytes into the composite SA/COL bioink and the investigation of important variables for cell proliferation and chondrogenesis. It could also be another potential strategy to mix electrospinning microtubes with SA/COL bioink for cartilage tissue engineering [44].

**Author Contributions:** Conceptualization, Y.Z.; Data curation, Y.C.; Formal analysis, Y.Z.; Funding acquisition, Y.Z.; Investigation, Y.C. and C.W.; Methodology, Y.Z.; Supervision, Y.Z.; Visualization, Y.C. and C.W.; Writing original draft, Y.C. and C.W.; Writing review & editing, Y.Z. and Y.C. All authors have read and agreed to the published version of the manuscript.

**Funding:** This research was funded by the start-up funds from Thomas J. Watson College of Engineering and Applied Science at the State University of New York at Binghamton, USA.

**Informed Consent Statement:** Not applicable.

**Acknowledgments:** Yingge Zhou would like to acknowledge the support from the ADL Small Grant (#ADL G217) from the Small Scale Systems Integration and Packaging (S3IP) Center of Excellence, funded by New York Empire State Development's Division of Science, Technology, and Innovation.

**Conflicts of Interest:** The authors declare no conflict of interest.

## References

1. Huang, Y.; Zhang, X.F.; Gao, G.; Yonezawa, T.; Cui, X. 3D Bioprinting and the Current Applications in Tissue Engineering. *Biotechnol. J.* **2017**, *12*, 1600734. [[CrossRef](#)]
2. Gu, B.K.; Choi, D.J.; Park, S.J.; Kim, Y.-J.; Kim, C.-H. 3D Bioprinting Technologies for Tissue Engineering Applications. In *Cutting-Edge Enabling Technologies for Regenerative Medicine*; Chun, H.J., Park, C.H., Kwon, I.K., Eds.; Advances in Experimental Medicine and Biology; Springer: Singapore, 2018; pp. 15–28.
3. Rider, P.; Kačarević, Ž.P.; Alkildani, S.; Retnasingh, S.; Barbeck, M. Bioprinting of Tissue Engineering Scaffolds. *J. Tissue Eng.* **2018**, *9*, 2041731418802090. [[CrossRef](#)] [[PubMed](#)]
4. Liu, F.; Chen, Q.; Liu, C.; Ao, Q.; Tian, X.; Fan, J.; Tong, H.; Wang, X. Natural Polymers for Organ 3D Bioprinting. *Polymers* **2018**, *10*, 1278. [[CrossRef](#)] [[PubMed](#)]
5. Peppas, N.A.; Hilt, J.Z.; Khademhosseini, A.; Langer, R. Hydrogels in Biology and Medicine: From Molecular Principles to Bionanotechnology. *Adv. Mater.* **2006**, *18*, 1345–1360. [[CrossRef](#)]
6. Yuan, H.; Zheng, X.; Liu, W.; Zhang, H.; Shao, J.; Yao, J.; Mao, C.; Hui, J.; Fan, D. A Novel Bovine Serum Albumin and Sodium Alginate Hydrogel Scaffold Doped with Hydroxyapatite Nanowires for Cartilage Defects Repair. *Colloids Surf. B Biointerfaces* **2020**, *192*, 111041. [[CrossRef](#)] [[PubMed](#)]
7. Miguel, S.P.; Cabral, C.S.D.; Moreira, A.F.; Correia, I.J. Production and Characterization of a Novel Asymmetric 3D Printed Construct Aimed for Skin Tissue Regeneration. *Colloids Surf. B Biointerfaces* **2019**, *181*, 994–1003. [[CrossRef](#)] [[PubMed](#)]
8. Zin, M.H.; Abdan, K.; Norizan, M.N. 1—The Effect of Different Fiber Loading on Flexural and Thermal Properties of Banana/Pineapple Leaf (PALF)/Glass Hybrid Composite. In *Structural Health Monitoring of Biocomposites, Fibre-Reinforced Composites and Hybrid Composites*; Jawaid, M., Thariq, M., Saba, N., Eds.; Woodhead Publishing Series in Composites Science and Engineering; Woodhead Publishing: Sawston, UK, 2019; pp. 1–17.

9. An, D.; Ji, Y.; Chiu, A.; Lu, Y.-C.; Song, W.; Zhai, L.; Qi, L.; Luo, D.; Ma, M. Developing Robust, Hydrogel-Based, Nanofiber-Enabled Encapsulation Devices (NEEDs) for Cell Therapies. *Biomaterials* **2015**, *37*, 40–48. [[CrossRef](#)]
10. Nair, L.S.; Laurencin, C.T. Biodegradable Polymers as Biomaterials. *Prog. Polym. Sci.* **2007**, *32*, 762–798. [[CrossRef](#)]
11. Chan, L.W.; Jin, Y.; Heng, P.W.S. Cross-Linking Mechanisms of Calcium and Zinc in Production of Alginate Microspheres. *Int. J. Pharm.* **2002**, *242*, 255–258. [[CrossRef](#)]
12. Yoon, Y.; Kim, C.H.; Lee, J.E.; Yoon, J.; Lee, N.K.; Kim, T.H.; Park, S.-H. 3D Bioprinted Complex Constructs Reinforced by Hybrid Multilayers of Electrospun Nanofiber Sheets. *Biofabrication* **2019**, *11*, 025015. [[CrossRef](#)]
13. Bociaga, D.; Bartniak, M.; Grabarczyk, J.; Przybyszewska, K. Sodium Alginate/Gelatine Hydrogels for Direct Bioprinting—The Effect of Composition Selection and Applied Solvents on the Bioink Properties. *Materials* **2019**, *12*, 2669. [[CrossRef](#)] [[PubMed](#)]
14. Mondal, A.; Gebeyehu, A.; Miranda, M.; Bahadur, D.; Patel, N.; Ramakrishnan, S.; Rishi, A.K.; Singh, M. Characterization and Printability of Sodium Alginate-Gelatin Hydrogel for Bioprinting NSCLC Co-Culture. *Sci. Rep.* **2019**, *9*, 19914. [[CrossRef](#)] [[PubMed](#)]
15. Wu, Z.; Li, Q.; Xie, S.; Shan, X.; Cai, Z. In Vitro and in Vivo Biocompatibility Evaluation of a 3D Bioprinted Gelatin-Sodium Alginate/Rat Schwann-Cell Scaffold. *Mater. Sci. Eng. C* **2020**, *109*, 110530. [[CrossRef](#)] [[PubMed](#)]
16. Seok, J.M.; Oh, S.H.; Lee, S.J.; Lee, J.H.; Kim, W.D.; Park, S.-H.; Nam, S.Y.; Shin, H.; Park, S.A. Fabrication and Characterization of 3D Scaffolds Made from Blends of Sodium Alginate and Poly(Vinyl Alcohol). *Mater. Today Commun.* **2019**, *19*, 56–61. [[CrossRef](#)]
17. Kumar, A.; Matar, I.A.I.; Han, S.S. 3D Printable Carboxylated Cellulose Nanocrystal-Reinforced Hydrogel Inks for Tissue Engineering. *Biofabrication* **2020**, *12*, 025029. [[CrossRef](#)]
18. Lee, J.M.; Suen, S.K.Q.; Ng, W.L.; Ma, W.C.; Yeong, W.Y. Bioprinting of Collagen: Considerations, Potentials, and Applications. *Macromol. Biosci.* **2021**, *21*, 2000280. [[CrossRef](#)]
19. Hospodiuk, M.; Dey, M.; Sosnoski, D.; Ozbolat, I.T. The Bioink: A Comprehensive Review on Bioprintable Materials. *Biotechnol. Adv.* **2017**, *35*, 217–239. [[CrossRef](#)]
20. Isaacson, A.; Swioklo, S.; Connon, C.J. 3D Bioprinting of a Corneal Stroma Equivalent. *Exp. Eye Res.* **2018**, *173*, 188–193. [[CrossRef](#)]
21. Wu, Z.; Su, X.; Xu, Y.; Kong, B.; Sun, W.; Mi, S. Bioprinting Three-Dimensional Cell-Laden Tissue Constructs with Controllable Degradation. *Sci. Rep.* **2016**, *6*, 24474. [[CrossRef](#)]
22. Yang, X.; Lu, Z.; Wu, H.; Li, W.; Zheng, L.; Zhao, J. Collagen-Alginate as Bioink for Three-Dimensional (3D) Cell Printing Based Cartilage Tissue Engineering. *Mater. Sci. Eng. C* **2018**, *83*, 195–201. [[CrossRef](#)]
23. Orth, P.; Gao, L.; Madry, H. Microfracture for Cartilage Repair in the Knee: A Systematic Review of the Contemporary Literature. *Knee Surg. Sports Traumatol. Arthrosc.* **2020**, *28*, 670–706. [[CrossRef](#)] [[PubMed](#)]
24. Donoso, R.; Figueroa, D.; Espinoza, J.; Yañez, C.; Saavedra, J. Osteochondral Autologous Transplantation for Treating Patellar High-Grade Chondral Defects: A Systematic Review. *Orthop. J. Sports Med.* **2019**, *7*, 2325967119876618. [[CrossRef](#)] [[PubMed](#)]
25. Kraeutler, M.J.; Belk, J.W.; Purcell, J.M.; McCarty, E.C. Microfracture Versus Autologous Chondrocyte Implantation for Articular Cartilage Lesions in the Knee: A Systematic Review of 5-Year Outcomes. *Am. J. Sports Med.* **2018**, *46*, 995–999. [[CrossRef](#)] [[PubMed](#)]
26. Shie, M.Y.; Chang, W.C.; Wei, L.-J.; Huang, Y.-H.; Chen, C.-H.; Shih, C.-T.; Chen, Y.-W.; Shen, Y.-F. 3D Printing of Cytocompatible Water-Based Light-Cured Polyurethane with Hyaluronic Acid for Cartilage Tissue Engineering Applications. *Materials* **2017**, *10*, 136. [[CrossRef](#)] [[PubMed](#)]
27. Camarero-Espinosa, S.; Calore, A.; Wilbers, A.; Harings, J.; Moroni, L. Additive Manufacturing of an Elastic Poly(Ester)Urethane for Cartilage Tissue Engineering. *Acta Biomater.* **2020**, *102*, 192–204. [[CrossRef](#)] [[PubMed](#)]
28. Sadeghianmaryan, A.; Naghieh, S.; Alizadeh Sardroud, H.; Yazdanpanah, Z.; Afzal Soltani, Y.; Sernaglia, J.; Chen, X. Extrusion-Based Printing of Chitosan Scaffolds and Their in Vitro Characterization for Cartilage Tissue Engineering. *Int. J. Biol. Macromol.* **2020**, *164*, 3179–3192. [[CrossRef](#)]
29. Hong, H.; Seo, Y.B.; Kim, D.Y.; Lee, J.S.; Lee, Y.J.; Lee, H.; Ajiteru, O.; Sultan, M.T.; Lee, O.J.; Kim, S.H.; et al. Digital Light Processing 3D Printed Silk Fibroin Hydrogel for Cartilage Tissue Engineering. *Biomaterials* **2020**, *232*, 119679. [[CrossRef](#)]
30. Du, Y.; Liu, H.; Yang, Q.; Wang, S.; Wang, J.; Ma, J.; Noh, I.; Mikos, A.G.; Zhang, S. Selective Laser Sintering Scaffold with Hierarchical Architecture and Gradient Composition for Osteochondral Repair in Rabbits. *Biomaterials* **2017**, *137*, 37–48. [[CrossRef](#)]
31. Kim, S.H.; Kim, D.Y.; Lim, T.H.; Park, C.H. Silk Fibroin Bioinks for Digital Light Processing (DLP) 3D Bioprinting. In *Bioinspired Biomaterials: Advances in Tissue Engineering and Regenerative Medicine*; Chun, H.J., Reis, R.L., Motta, A., Khang, G., Eds.; Springer: Singapore, 2020; pp. 53–66.
32. Rathan, S.; Dejob, L.; Schipani, R.; Haffner, B.; Möbius, M.E.; Kelly, D.J. Fiber Reinforced Cartilage ECM Functionalized Bioinks for Functional Cartilage Tissue Engineering. *Adv. Healthc. Mater.* **2019**, *8*, 1801501. [[CrossRef](#)]
33. Al-Sabah, A.; Burnell, S.E.A.; Simoes, I.N.; Jessop, Z.; Badiei, N.; Blain, E.; Whitaker, I.S. Structural and Mechanical Characterization of Crosslinked and Sterilised Nanocellulose-Based Hydrogels for Cartilage Tissue Engineering. *Carbohydr. Polym.* **2019**, *212*, 242–251. [[CrossRef](#)]
34. Gong, Y.; Wang, F.; Al-Furjan, M.S.H.; Shan, L.; He, J.; Bian, X.; Bi, Z.; Liu, H.; Li, W.; Shao, H.; et al. Experimental Investigation and Optimal 3D Bioprinting Parameters of SA-Gel Porous Cartilage Scaffold. *Appl. Sci.* **2020**, *10*, 768. [[CrossRef](#)]
35. Isaeva, E.V.; Beketov, E.E.; Yuzhakov, V.V.; Arguchinskaya, N.V.; Kisel, A.A.; Malakhov, E.P.; Lagoda, T.S.; Yakovleva, N.D.; Shegai, P.V.; Ivanov, S.A.; et al. The Use of Collagen with High Concentration in Cartilage Tissue Engineering by Means of 3D-Bioprinting. *Cell Tiss. Biol.* **2021**, *15*, 493–502. [[CrossRef](#)]

36. Osidak, E.O.; Kozhukhov, V.I.; Osidak, M.S.; Domogatsky, S.P. Collagen as Bioink for Bioprinting: A Comprehensive Review. *Int. J. Bioprint.* **2020**, *6*, 270.
37. Belalia, F.; Djelali, N.E. Rheological Properties of Sodium Alginate Solutions. *Rev. Roum. Chim* **2014**, *59*, 2.
38. Ribeiro, A.; Blokzijl, M.M.; Levato, R.; Visser, C.W.; Castilho, M.; Hennink, W.E.; Vermonden, T.; Malda, J. Assessing Bioink Shape Fidelity to Aid Material Development in 3D Bioprinting. *Biofabrication* **2017**, *10*, 014102. [[CrossRef](#)]
39. Habib, A.; Khoda, B. Development of Clay Based Novel Hybrid Bio-Ink for 3D Bio-Printing Process. *J. Manuf. Process.* **2019**, *38*, 76–87. [[CrossRef](#)]
40. Schwab, A.; Levato, R.; D'Este, M.; Piluso, S.; Eglin, D.; Malda, J. Printability and Shape Fidelity of Bioinks in 3D Bioprinting. *Chem. Rev.* **2020**, *120*, 11028–11055. [[CrossRef](#)]
41. Cao, P.; Tao, L.; Gong, J.; Wang, T.; Wang, Q.; Ju, J.; Zhang, Y. 4D Printing of a Sodium Alginate Hydrogel with Step-Wise Shape Deformation Based on Variation of Crosslinking Density. *ACS Appl. Polym. Mater.* **2021**, *3*, 6167–6175. [[CrossRef](#)]
42. Boddupalli, A.M.; Bratlie, K. Second Harmonic Generation Microscopy of Collagen Organization in Tunable, Environmentally Responsive Alginate Hydrogels. *Biomater. Sci.* **2019**, *7*, 1188–1199. [[CrossRef](#)] [[PubMed](#)]
43. You, C.; Xiong, X.; Liu, X.; Cui, R.; Wang, C.; Zhao, G.; Zhi, W.; Lu, M.; Duan, K.; Weng, J.; et al. 3D Bioprinting of Shear-Thinning Hybrid Bioinks with Excellent Bioactivity Derived from Gellan/Alginate and Thixotropic Magnesium Phosphate-Based Gels. *J. Mater. Chem. B* **2020**, *8*, 5500–5514.
44. Tan, G.; Zhou, Y.; Sooriyaarachchi, D. Musculoskeletal Tissue Engineering Using Fibrous Biomaterials. In *Wound Regeneration: Methods and Protocols*; Das, H., Ed.; Methods in Molecular Biology; Springer: New York, NY, USA, 2021; pp. 31–40.